UNICA UNIVERSITÀ DEGLI STUDI DI CAGLIARI

LOW CO_2 EMISSIONS CHEMICALLY RECUPERATED GAS TURBINES FED BY RENEWABLE METHANOL

[a*] *Vittorio Tola*, [a] *Francesco Lonis*
[a]University of Cagliari, Department of Mechanical Chemical and of Materials Engineering, Via Marengo 2, Cagliari, Sardinia, Italy

*Corresponding author e-mail: vittorio.tola@dimcm.unica.it +390706755102

Abstract

Steam reforming of the fuel in chemically recuperated gas turbine (CRGT) plants allows to perform a heat recovery of the gas turbine exhausts, boosting the plant performance. Power-to-liquids technologies are a very interesting solution for storing the excess of renewable electricity into liquid fuels. Among the renewable fuels, methanol is well-known as a hydrogen carrier and an energy feedstock. Indeed, methanol can be stored, transported and used in an easier way than hydrogen.

In this paper a CRGT fed by renewable methanol produced in power-to-liquids plant through the CO_2 hydrogenation process was studied. The hydrogen needed to synthesize methanol is produced in an alkaline electrolyser, while the CO_2 is captured from the CRGT exhausts. The opportunity of introducing an organic Rankine cycle (ORC) to enhance the energy production was also investigated. Dedicated simulation models of the single sections and of the overall system were developed through the commercial software Aspen Plus.

The overall system was sized to generate about 350 kg/h of methanol, resulting in a power production in the order of 600-750 kW. The study demonstrated that the integrated system based on a CRGT plant fed by renewable methanol can effectively store RES surplus and produce electricity with very low CO_2 emissions. The overall system shows a power-to-power efficiency of about 0.23 that can be slightly increased with the introduction of an ORC system to better exploit the heat released by the CRGT.

Keywords

Chemically recuperated gas turbine, power-to-liquids, renewable methanol, methanol synthesis section, CO_2 hydrogenation, CO_2 capture.

Nomenclature

AEL	Alkaline electrolyser
BOP	Balance of plant
CRGT	Chemically recuperated gas turbine
MEA	Monoethanolamine
MSS	Methanol synthesis section
ORC	Organic Rankine cycle
RES	Renewable energy sources
TIT	Turbine inlet temperature

1. Introduction

Nowadays, climate change appears to be one of the main challenges to be faced, requiring a large effort to reduce greenhouse gases emissions. In this framework, the combination of renewable energy exploitation and carbon capture is a key solution to make the energy systems as "green" as possible [1]. Among the main available energy systems, gas turbines are surely one of the most environmentally friendly, since they can be fuelled by clean gaseous fuels, such as natural gas, reducing emissions of pollutants and greenhouses gases [2]. Moreover, gas turbines power plants can be equipped with a CO_2 capture section, removing a great amount of CO_2 from the exhausts [3]. The thermo-chemical recovery of the exhausts heat through the steam reforming of the fuel is an interesting option to increase the performance of a gas turbine plant (chemically recuperated gas turbine, CRGT) [4,5]. Usually, the steam reforming processes involve the use of methane. Nevertheless, in case of CRGT power plants, the steam reforming of methane leads to significant drawbacks, since the methane reforming temperature (600–800 °C) is notably higher than the exhaust temperature of commercial gas turbines [6–8]. On the contrary, alternative fuels, such as methanol, can be more suitable for CRGT power plants, owing to their lower reforming temperature (250–300 °C for the methanol) [9,10]. Methanol is a promising energy carrier because it can be easily stored, transported and used without significant changes in the existing infrastructure [11]. Typically, methanol is produced from fossil fuels, but renewable methanol can be also obtained via the application of power-to-X technologies [12], exploiting hydrogen, synthesised from the excess of renewable energy sources (RES), and recycled CO_2, following

special conversion routes, such as the catalytic CO_2 hydrogenation process [13,14]. The power-to-X approach is one of the most promising candidates in the context of clean renewable fuels and it can be employed not only to produce methanol, but also a variety of other fuels and chemical compounds, such as methane, dimethyl ether, syngas, and conventional fuels (i.e. gasoline, diesel fuel, kerosene, and jet fuel) [15–17]. In addition, power-to-X could lead to the independency from fossil fuels, while boosting RES efficiency and penetration [18,19]. Indeed, the large penetration of electricity production from RES calls for the diffusion of energy storage systems boosting RES reliability [20–22]. Since power-to-X technologies allows the storage of excess renewable energy in long-term and high-energy density storage systems, a strong interest in this field has been developed in the last years as reported in Chehade et al. [23], which reviewed the power-to-X demonstration projects carried out around the world. Kourkoumpas et al. [24] carried out a techno-economic analysis of a power-to-methanol concept, exploiting CO_2 recycled from lignite power plants. They found that this technology would be cost competitive (421 €/ton and 380 €/ton in the Greek and German market, respectively) compared to conventional methanol production. González-Aparicio et al. [25] analysed the optimal operating conditions of a power-to-methanol system fed by wind to reduce forecasting uncertainty and improve the revenues deriving from renewable energy or methanol selling. Adnan and Kibria [26] carried out a comparative techno-economic and life-cycle assessment of different power-to-methanol synthesis pathways, finding a competitive cost of around 430-435 $/ton under an optimistic scenario. An innovative work by Bos et al. [27] studied a wind power-to-methanol plant employing RES, electrolysis of water and CO_2 air capture, finding a total conversion efficiency of 50% with a reasonable cost of 750-800 €/ton for such an innovative concept. Crivellari et al. [28–30] carried out a variety of works on power-to-X, exploiting offshore renewable energy.

A few works focused on the analysis of a CRGT fuelled by alternative fuels, such as methanol or dimethyl ether, are found in literature. Carapellucci et al. [5] analysed the performance of two methanol fuelled CRGT belonging to two different technological classes. The main finding of the work is that CRGT fuelled by methanol can achieve higher performance, both reducing the emissions of different pollutants (i.e., NO_X and N_2O) and maintaining the same level of CO emissions than conventional gas turbines. Cocco et al. [9] analysed the performance of an aeroderivative gas turbine by replacing the natural gas with pure or fuel-grade dimethyl ether, and methanol. The authors found out that the performance improves with the use of both DME and methanol compared to the natural gas. In particular, introducing the chemical recuperation of

DME significantly improves the power output by about 45% in comparison to the reference plant fed by natural gas. Alves and Nebra [31] made an analysis and nonlinear optimization of a CRGT cycle in order to investigate the temperature and pressure influence on the global performance. The optimal solution was found achieving both the highest inlet temperature of the turbine and the highest compression ratio in the air compressor. A thermodynamic second law analysis was also performed for detecting the greatest sources of irreversibility. Liu et al. [32] considered a distributed energy system based on the integration between a CRGT fuelled by methanol and a solar thermo-chemical process. The synthesis gas obtained from the methanol reforming process feeds a micro gas turbine integrated in a distributed energy system to deliver output cooling, heating, and power. The overall system showed a remarkably high primary energy efficiency of 70%, thanks to the coupling of the solar field and the chemical recuperation. Cherednichenko et al. [33] estimated both the economic efficiency and the carbon dioxide emissions of a chemically recuperated gas turbine fed by methanol and ethanol. At the optimal water to methanol ratio of 3, the CRGT can increase the efficiency by 4% and reduce tank-to-wake emissions by 80%.

Moreover, some papers investigated the integration of the CRGT with different process and peculiar applications. Florez-Orrego et al. [34] recovered the exergy available from the auto-thermal reformer effluent through a syngas production, while Luo et al. [35] integrated a CRGT cycle with a thermal seawater desalination process. Pan et al. [36] investigated operational rules and control strategies of the chemically recuperated gas turbines fuelled by diesel for naval applications. Su et al. [37] proposed a biogas-fired CHP based on chemically recuperated gas turbine cycle. Ni et al. [38] proposed a thermodynamic analysis of a solar-assisted chemically recuperated gas turbine plant with a two-stage fuel steam reforming.

In this paper a performance assessment of an integrated plant based on a power-to-liquids system and a low CO_2 emissions CRGT fuelled by methanol is presented. Methanol is produced in a methanol synthesis section (MSS) via catalytic CO_2 hydrogenation [39], it is stored and reused by producing electricity via the CRGT to level out peak demands. The required hydrogen is produced in an alkaline electrolyser (AEL), exploiting the excess of electricity generated from RES, while the CO_2 is captured from the CRGT exhausts. In order to better exploit the residual heat released by the CRGT, an integration between the overall system and an organic Rankine cycle (ORC) was also investigated. Heat recovery and thermal integration of the overall system are performed to obtain optimal operating conditions and energy savings in each section. Performance energy indexes were

also defined to evaluate the performance of the single sections and of the overall system. Functional schemes and dedicated simulation models were implemented using the commercial software Aspen Plus.

Numerous studies on power-to-power plants based on renewable methanol can be found in literature. However, the proposed plants are usually based on fuel cells [40–43]. To the best of authors' knowledge, the analysis of a CRGT plant coupled to clean hydrogen production and methanol synthesis from captured CO_2 has not yet been analysed in literature. This research gap should be faced to allow using renewable methanol in a small-term perspective, feeding a more commercial system as a gas turbine. In fact, fuel cells lead to a higher overall efficiency, but are characterized by sensibly higher costs and could be competitive in a medium-term perspective. The comprehensive investigation carried out through parametric analysis shows the optimal conditions, where the best synergy between the CRGT and the ORC is achieved. The chosen configuration of the plant, combining clean hydrogen produced from RES and CO_2 captured from the turbine exhausts, determines a closed cycle, where the same CO_2 is used indefinitely to produce the methanol feeding the gas turbine.

2. System configuration and methodology

The general configuration of the overall system mainly includes the following sections:

- an alkaline water electrolyser,
- a methanol synthesis and purification section,
- a methanol storage system,
- a chemically recuperated gas turbine plant integrated with a CO_2 capture system,
- an organic Rankine cycle (optional).

Figure 1 shows the functional scheme of the overall system.

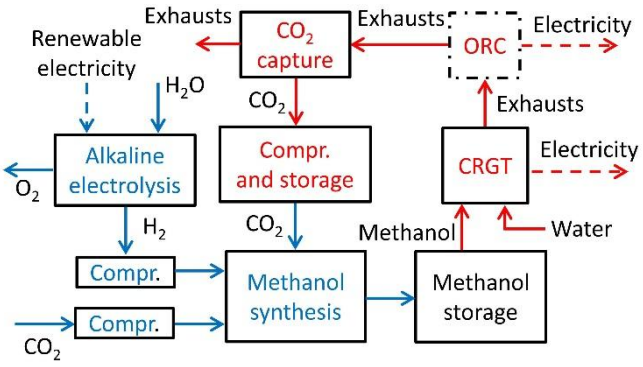

Fig. 1 – Functional scheme of the overall system

In case of excess electricity from RES sources, an alkaline electrolyser (AEL) transforms feeding water into oxygen and hydrogen. Hydrogen is compressed and feeds, together with CO_2, a synthesis section, where methanol is produced in a catalytic reactor (charge phase, blue), following the CO_2 hydrogenation process. Then, methanol is stored at ambient conditions, for later feeding a CRGT in case of higher electricity demand from the user (discharge phase). The heat released by the CRGT exhausts is exploited in the reforming section, where the water-methanol mixture is preheated, vaporized, superheated, and reformed, as well as in the CO_2 capture section, according to the scheme shown in Figure 2.

Fig. 2 – Simplified scheme of the exhausts heat recovery

ECO (Economizer), RBL (Reboiler), RFR (Reformer), SH (Superheater), VAP (Vaporizer)

Firstly, the heat recovery from the exhausts allows performing the endothermic reforming reactions (RFR). Then, the exhausts are used for the water-methanol mixture superheating (SH), vaporizing (VAP), and partially preheating at high temperature (ECO-HT). Subsequently, the exhausts provide the thermal energy to regenerate the solvent (monoethanolamine, MEA) inside the reboiler of the CO_2 removal section (RBL). Finally, exhausts heat is absorbed by a low-temperature preheating of the water-methanol mixture (ECO-LT). Downstream of the CRGT, an ORC power plant can be also introduced. The ORC partially exploits the thermal energy of the exhaust gases, reducing the amount of heat available for the reforming processes, but boosting the performance of the overall system.

The overall system was sized with reference to a 3.2 MW commercial AEL [44]. Such an electrolyser assures a hydrogen production slightly higher than 800 Nm^3/h (approximately 71.5 kg/h), requiring a water flow rate of about 640 kg/h and generating about 350 kg/h of methanol in the MSS (about half of the production of the only existing commercial renewable methanol plant, the Icelander George Olah Plant [45]). Assuming the same duration for the charge and discharge phases, such a methanol production results in a power production in the order of 600-750 kW, depending on the CRGT operation parameters.

2.1 Alkaline electrolyser

Among the electrolysis processes, low temperature alkaline electrolysis of water was chosen for this application, since it is a largely diffused and commercially available technology [46]. Inside the AEL the electrolyte is based on a liquid solution of KOH or NaOH. In this study, the model of the alkaline electrolyser was implemented in Aspen Plus through specified user-defined blocks, employing the Ideal properties method. The electrochemical model was developed adapting the equations provided by Ursua and Sanchis [47] for the simulation of commercial water AELs. Figure 3 shows a simplified functional scheme of the AEL as modelled in Aspen Plus.

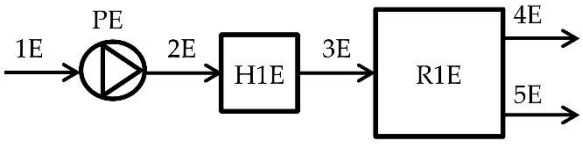

Fig. 3 – Simplified functional scheme of the alkaline electrolyser

Feeding water (1E) is pumped (PE) and heated (H1E) to the cell (R1E) operating conditions. Since the cell operates at low temperature, the operating voltage is above the thermo-neutral voltage, leading to a heat production by the Joule effect that can be employed to preheat the feed water, without any external source. Inside the cell, hydrogen (4E) and oxygen (5E) are produced from water (3E). The reactor was modelled as a stoichiometric reactor.

The nominal current of the alkaline electrolyser is equal to 120 A, while the net voltage E_{AEL} is calculated adding to the equilibrium potential E_{eq} the overvoltages caused by the ohmic and activation resistances as shown in Eq. (1):

$$E_{AEL} = E_{eq} + \left[V_{ohm} + V_{act,an} + V_{act,cat}\right] \quad (1)$$

where V_{ohm} is the ohmic overvoltage, $V_{act,an}$ and $V_{act,cat}$ are the anodic and cathodic activation resistances, respectively. The equilibrium potential is expressed as a function of temperature and pressure according to Eq. (2)

$$E_{eq} = N_S \left[E_0 + \frac{RT_c}{2F} ln\left(\frac{(p-p_{v,KOH})(p-p_{v,KOH})^{\frac{1}{2}}}{a_{H_2O,KOH}}\right)\right] \quad (2)$$

where N_S is the number of cells of one stack, E_0 is the reversible potential of a single cell; p and $p_{v,KOH}$ are the stack operating pressure and the vapour pressure of the KOH solution, while $a_{H_2O,KOH}$ is the water activity in the KOH solution.

The reversible potential E_0 is calculated according to Eq. (3):

$$E_0 = 1.5184 - 1.5421 \times 10^{-3}\, T_c + 9.526 \times 10^{-5}\, T_c\ ln(T_c) + 9.84 \times 10^{-8}\, T_c^2 \quad (3)$$

where T_c is the operating temperature of the cell.

A validation of the AEL model was presented in Lonis [43,48].

For a given cell temperature, a higher operating pressure increases the AEL power requirements, reducing the efficiency. Nevertheless, a higher pressure in the AEL reduces the power required by the hydrogen compressors in the methanol synthesis section.

2.2 Methanol synthesis section

The hydrogen produced by the AEL feeds the methanol synthesis section for producing the liquid methanol used to store energy. The section is mainly composed of:

- two compressor trains for hydrogen and CO_2,
- an adiabatic synthesis reactor for the methanol production,
- a distillation column for the methanol purification.

The methanol is produced through a CO_2 hydrogenation process in an adiabatic catalytic reactor. In particular, the overall process of the methanol production is based on the following three reactions: the water gas shift reaction (4), the CO hydrogenation reaction (5), the CO_2 hydrogenation reaction (6).

$$CO_2 + H_2 \rightleftarrows CO + H_2O \quad (4)$$

$$CO + 2H_2 \rightleftarrows CH_3OH \quad (5)$$

$$CO_2 + 3H_2 \rightleftarrows CH_3OH + H_2O \quad (6)$$

The methanol synthesis process was simulated through an LHHW kinetic model, specifically developed in the Aspen Plus environment [39,49]. Various properties methods were used, depending on the different sub-processes analyzed (e.g., SRK for the reactor, NTRL-SK for the distillation column). An extensive description of the kinetic model of the reactor can be found in Lonis et al. [42].

Figure 4 shows the simplified functional scheme of the methanol synthesis and purification section.

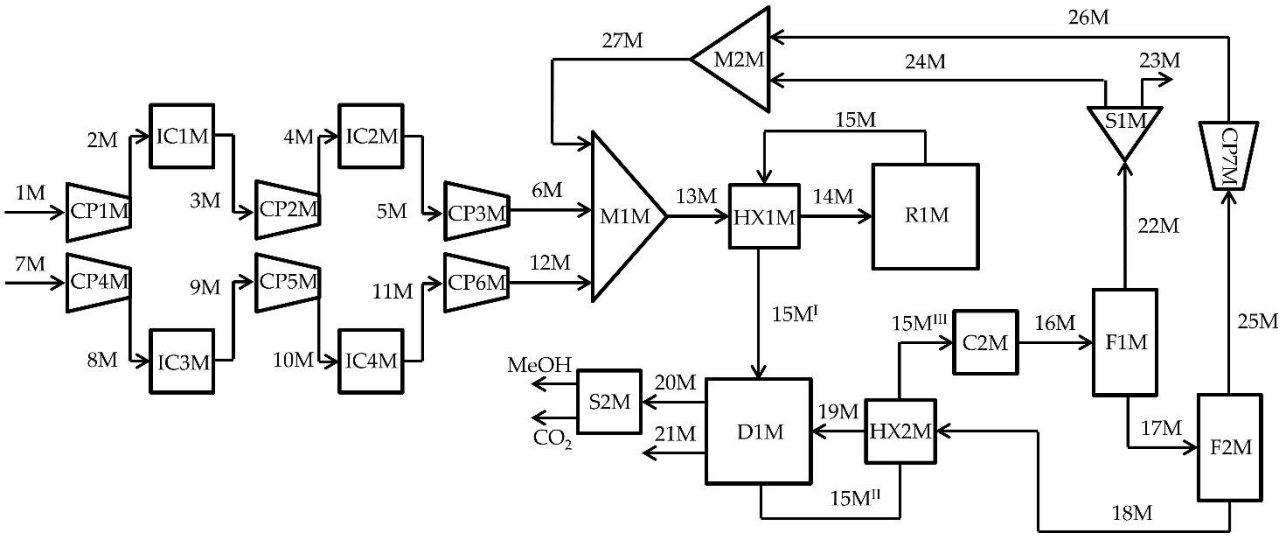

Fig. 4 – Simplified functional scheme of the methanol synthesis and purification section
C (Cooler), CP (Compressor), D (Distillation column), F (Flash), H (Heater), C (Intercooler), M (Mixer), R (Reactor), S (Splitter)

Hydrogen (1M) and CO_2 (7M) are compressed to the operating pressure of the synthesis reactor (R1M) (set to 65 bar [39]), by means of three intercooled compressors. Then, H_2 (6M) and CO_2 (12M) are mixed with the re-circulated gases (27M) and preheated (H1M) to the reactor inlet temperature

(set to 210 °C [39]). Due to the high rate of recirculation, the products of the synthesis process are mainly composed of hydrogen and CO_2, with only a small content of methanol, water vapour and CO. Due to the exothermicity of the CO_2 hydrogenation reaction a large amount of thermal energy is available in the products and it is used: a) to preheat the reactor feeding (HX1M), b) to provide the reboiling duty to the distillation column (D1M), and c) to preheat the methanol to be purified (HX2M). Later, the temperature of the products is further reduced with an external cooler (C2M), reaching the operating conditions of two flash processes (F1M and F2M). The first flash occurs at 65 bar and 50 °C, the latter at 1.2 bar and 22 °C. The flash processes boost the production of methanol, recycling back to the reactor the incondensable gases (22M and 25M). The liquid product (18M), namely crude methanol, is mainly composed of methanol and water (both about 49% by vol.), with a small amount of CO_2. The crude methanol is treated in the purification section, where a distillation column (D1M) separates water and methanol, boosting the methanol purity. In fact, the methanol and CO_2 are distilled at the top of the column (20M) and then are easily separated by condensing the former.

2.3 Chemically recuperated gas turbine

The CRGT power plant is based on a gas turbine and a reforming section where the water-methanol mixture is converted into a gas inside a catalytic reformer. In this study, the CRGT is also integrated with a post-combustion CO_2 removal section, based on a mixture of water and MEA (30%wt). A simplified functional scheme of the CRGT power plant is shown in Figure 5.

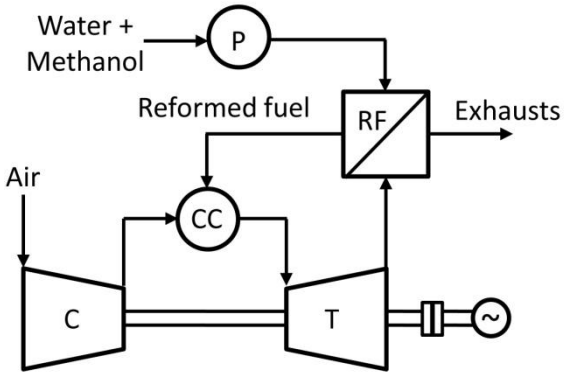

Fig. 5 – Simplified functional scheme of the CRGT power plant

C (Compressor), CC (Combustion chamber), P (Pump), RF (Reforming section), T (turbine)

Since the methanol production from the MSS is quite small (lower than 0.1 kg/s), the CRGT power plant here analysed is based on a small-size gas turbine (in the order of several hundred kW). Small-size gas turbines are characterized by a maximum temperature (TIT, turbine inlet temperature) in the range 900-1100 °C and by a pressure ratio β in the range 5-12 [50]. Main parameters of the selected gas turbine are reported on Table 1.

Table 1 Main parameters of the gas turbine	
Fuel mass flow (methanol)	0.0975 kg/s
Compression ratio, β	5-12
Turbine inlet temperature, TIT	900-1100°C
Compressor polytropic efficiency	0.86
Turbine polytropic efficiency	0.85
Inlet pressure drop (% of p_{IN})	1%
Combustion pressure drop (% of p_{IN})	3%
Exhaust pressure drop (% of p_{IN})	3%
Combustion efficiency	0.99
Mech. losses and aux. consumption	5%

Downstream of the gas turbine, the exhausts provide the heat required to preheat, vaporize, superheat and reform the water-methanol mixture. Since the reformed gas is characterized by both a density and an LHV considerably lower than those of the natural gas, a sensibly higher fuel flow rate is required. The high flow rate calls for a special design of the fuel feeding system, similarly to the gas turbines of IGCC, fed by a coal synthesis gas. In fact, gas turbines are designed to be fed with natural gas, consequently the increase of the mass flow rate from the compressor to the turbine is below 2-3%. For this reason, in this study, an increase of the mass flow rate equal to 20% was assumed as maximum tolerable value, to avoid problems of both combustion instability and compressor stall.

The performance assessment has been carried out with reference to different water/methanol molar ratios *n* entering the reforming section, because the composition of the reformed gas (mainly hydrogen, water and CO_2) strictly depends on it. The reforming pressure has been assumed accounting for the pressure ratio of the gas turbine and for the reforming section and combustor pressure drops (set equal to 5% and 3% of the inlet pressure, respectively). A reforming temperature guaranteeing an almost complete conversion of the methanol was considered for the analysis.

The methanol steam reforming process can be described by means of the reverse reactions than of the reactions (4), (5) and (6), namely the water gas shift conversion, the methanol decomposition,

and the methanol steam reforming. The methanol conversion rate depends on various operating parameters, in particular, temperature, pressure and *n*. Indeed, steam reforming of methanol is favoured by low pressure, high temperature and *n* values. Moreover, to avoid carbon formation a water/methanol molar ratio higher than the stoichiometric one (equal to 1) is required [10]. In addition, other parameters as the catalyst activity and the reformer configuration and geometry can be considered, taking into account the kinetic of the reactions. However, the methanol steam reforming reactions can be considered under equilibrium conditions in case of reforming temperature higher than 250-300 °C [11].

2.4 CO_2 capture section

The proposed CRGT plant is integrated with a CO_2 capture system. In case of CO_2 capture from flue gas at atmospheric pressure, the most appropriate choice is the chemical absorption with a solvent based on amines [51]. Among amines, MEA is the most suitable option [52], due its widespread availability, although in a near term future better solvents should achieve commercial readiness [53]. In fact, MEA is characterized by a high energy requirement for regeneration, causing a large penalization on performance. The model of the CO_2 capture section was developed on Aspen Plus environment, using the properties method Elecnrtl. Figure 6 shows a simplified scheme of the CO_2 removal section.

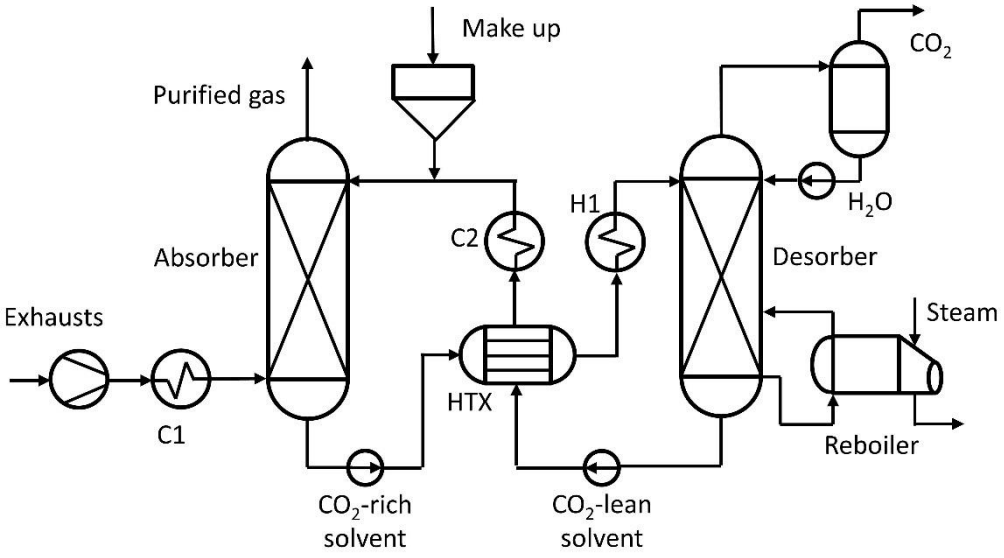

Fig. 6 – Simplified scheme of the CO_2 removal section

The CO_2 capture system is mainly based on two columns: an absorption one (absorber) for capturing the CO_2 from the flue gas and a regenerative one (desorber) for the thermal regeneration of the solvent rich in CO_2. Exhaust gas is cooled (C1) to about 40 °C and enters the absorber from the bottom, counter-current with the water-MEA solvent that absorbs a large amount of CO_2. The gas resulting from the CO_2 capture process (purified gas) is mainly composed of nitrogen, with a molar fraction of 80-85%, depending on both the air-to-methanol ratio feeding the combustion chamber and the CO_2 removal rate. The purified gas is discharged from the top of the column, while the CO_2-rich solvent is pumped and heated (HTX and H1) before feeding the desorber. Inside the regenerative column, a reboiler provides thermal energy, allowing the release of a large part of CO_2 and water vapour from the rich solvent. In the upper section a large fraction of water vapour condensates (H_2O), while the CO_2-rich flow (CO_2), with a purity of about 95%, is sent to the conditioning and compression section. The CO_2-lean solvent is extracted at the bottom of the column, pumped, cooled (HTX and C2), and recirculated back to the absorber. The main operating parameters of the CO_2 removal section are shown in Table 2.

Table 2 Main operating parameters of the CO_2 removal section	
Absorber temperature	35 °C
MEA mass fraction	30%
CO_2/MEA molar ratio in the lean solvent	0.28
Solvent/gas mass ratio	4.4

A CO_2 removal efficiency equal to 90% was assumed, as in typical post-combustion CO_2 removal systems based on amine. The reboiler heat requirement is supplied by low-pressure steam produced exploiting the CRGT exhaust thermal energy.

The CO_2 removal section is integrated with a proper conditioning and compression section to match requirements for CO_2 storage. In particular, a pressure of 8 MPa and a CO_2 purity above 99.5% were set. The CO_2 compression process is carried out through three intercooled compressors.

2.5 ORC section

The introduction of an ORC plant was considered to increase the power output of the system by exploiting the large residual heat of the CRGT exhaust gases. ORC systems are based on a Rankine cycle, with an organic fluid as working fluid. Differently from steam cycles, ORC systems can be fed

also by low-temperature heat (below 350 °C). Thanks to its relative simplicity, specific costs of an ORC are sensibly lower than those of a small-size steam plant [54,55]. Since the thermal energy from the CRGT is minor (allowing an ORC size lower than 100 kW_e), a simple configuration was chosen, with the ORC composed of an evaporator, a turbine, an air-cooled condenser, a pump, and a regenerator, as a simple single pressure level cycle [54]. The ORC model was developed on Aspen Plus environment using the properties method Peng-Robinson. Figure 7 shows a simplified functional scheme of the ORC plant.

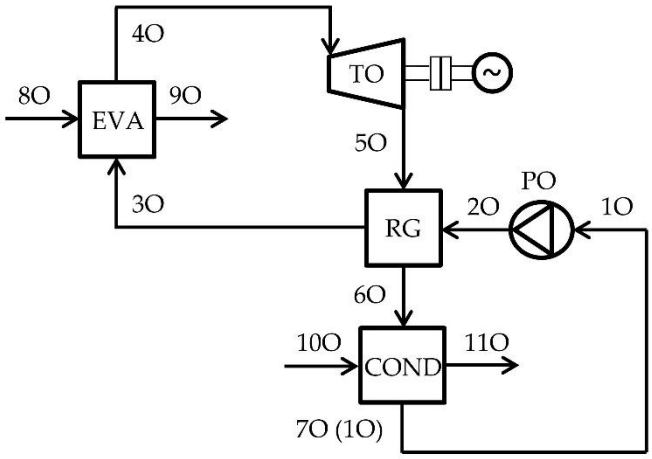

Fig. 7 – Simplified scheme of the ORC plant

The organic fluid, as subcooled liquid (1O), is pumped (PO) to the maximum pressure of the cycle (2O). Then, it is firstly preheated in the regenerator (RG), via the cooling of expanded fluid (5O) and, then, it is vaporized in the heat exchanger (EVA), exploiting the thermal energy of the CRGT exhausts (8O). The working fluid (4O) is characterized by some degrees of superheating and it expands to the minimum pressure of the cycle in the turbine (TO). Since the temperature of the turbine exhaust (5O) is relatively high, due to the shape of the T-s diagram for a typical organic fluid, the preheating of the organic fluid (2O) can be performed in the regenerator. Finally, ambient air (10O) allows the condensation and the sub-cooling of the organic fluid (7O) in the condenser (COND).

Despite its flammability and toxicity [56], benzene was chosen as organic fluid in this study, since, thanks to both its high critical pressure (48.9 bar) and low critical temperature (289 °C) [57], it well matches with the temperature of the hot source, providing the highest efficiency [58]. Table 3 summarizes the main operating parameters of the ORC

Table 3 Main parameters of the ORC plant

Working fluid	Benzene
Thermal power	50-500 kW
Turbine inlet temperature	290 °C
Cycle maximum pressure	46.5 bar
Cycle minimum temperature	44.5 °C
Cycle minimum pressure	0.35 bar
Minimum ΔT in COND and RG	10 °C
Mech. losses and aux. consumption	5%
Turbine isentropic efficiency	0.46-0.70*
Pump isentropic efficiency	0.7
Fan isentropic efficiency	0.75
Condenser air pressure drop	0.25 kPa
* Depending on the organic fluid mass flow	

Since the temperature of the hot source is higher than 300 °C, maximum cycle pressure and temperature were set to 46.5 bar and 290 °C. The presence of an air-cooled condenser leads to a relatively high value of the minimum temperature of the ORC cycle. In fact, assuming an air ambient temperature of 25 °C, a condensation temperature of about 48 °C was calculated, resulting in a minimum pressure at the condenser equal to 0.35 bar. A minimum temperature difference of 10 °C was set in both the regenerator and the condenser, as well as a subcooling of 3° C in the condenser. For small-size ORC the isentropic efficiency of the turbine is strictly related to the mass flow of the evolving organic fluid. A correlation by Macchi and Astolfi [54] was used to evaluate it for different thermal power available.

3. Performance Indexes

In the study of a such complex and integrated system is not unambiguous to evaluate the performance of the overall system. For this reason, a few performance indexes were defined to establish the performance of the subsystems and of the overall plant.

The electrolysis efficiency is defined as the chemical power of the produced hydrogen $\dot{m}_{H_2} \cdot LHV_{H_2}$ divided by the sum of the electric power consumed in the electrolysis process P_{AEL} and the auxiliaries power requirements $P_{BOP,AEL}$, as shown in Eq. (7):

$$\eta_{AEL} = \frac{\dot{m}_{H_2} \cdot LHV_{H_2}}{P_{AEL} + P_{BOP,AEL}} \quad (7)$$

For the methanol synthesis section both an actual overall efficiency η_{MSS} and a chemical energy conversion efficiency $\eta_{MSS,C}$ can be defined, as reported in Eq. (8) ad (9):

$$\eta_{MSS} = \frac{\dot{m}_{MeOH} \cdot LHV_{MeOH}}{\dot{m}_{H_2} \cdot LHV_{H_2} + P_{BOP,MSS}} \; ; \tag{8}$$

$$\eta_{MSS,C} = \frac{\dot{m}_{MeOH} \cdot LHV_{MeOH}}{\dot{m}_{H_2} \cdot LHV_{H_2}} \tag{9}$$

where $\dot{m}_{MeOH} \cdot LHV_{MeOH}$ is the chemical power of the methanol. The actual overall efficiency also considers the contribution of MSS auxiliaries $P_{BOP,MSS}$, while the chemical energy conversion efficiency does not.

An efficiency of the power-to-liquids process η_{PtL}, is obtained considering the efficiency chain of the electrolysis and MSS as shown in Eq. (10):

$$\eta_{PtL} = \frac{\dot{m}_{MeOH} \cdot H_{i,MeOH}}{P_{AEL} + P_{BOP,AEL} + P_{BOP,MSS}} = \eta_{AEL} \cdot \varphi_{AEL} \cdot \eta_{MSS,C} \tag{10}$$

where the term φ_{AEL} represents the fraction of power entering the AEL with respect to the total power (Eq. (11)):

$$\varphi_{AEL} = \frac{P_{AEL} + P_{BOP,AEL}}{P_{AEL} + P_{BOP,AEL} + P_{BOP,MSS}} \tag{11}$$

The efficiency of the electricity production, the net power divided by the methanol chemical power, can be defined taking into account or not the ORC plant, as shown in Eqs. (12) and (13):

$$\eta_{CRGT} = \frac{P_{CRGT} - P_{BOP,CRGT}}{\dot{m}_{MeOH} \cdot LHV_{MeOH}} \; ; \tag{12}$$

$$\eta_{CRGT+ORC} = \frac{P_{CRGT} + P_{ORC} - P_{BOP,CRGT} - P_{BOP,ORC}}{\dot{m}_{MeOH} \cdot LHV_{MeOH}} \tag{13}$$

Globally, the power-to-power efficiency of the overall system η_g can be defined as the ratio between the net power produced and the total power entering the overall system, as shown in Eqs. (14) and (15).

$$\eta_g = \frac{P_{CRGT} - P_{BOP,CRGT}}{P_{AEL} + P_{BOP,AEL} + P_{BOP,MSS}} = \eta_{PtL} \cdot \eta_{CRGT} \; ; \tag{14}$$

$$\eta_g = \frac{P_{CRGT} + P_{ORC} - P_{BOP,CRGT} - P_{BOP,ORC}}{P_{AEL} + P_{BOP,AEL} + P_{BOP,MSS}} = \eta_{PtL} \cdot \eta_{CRGT+ORC} \tag{15}$$

4. Results and discussion

The proposed power-to-liquids system is characterized by an efficiency η_{PtL} slightly lower than 0.58, due to an electrolysis efficiency η_{AEL} of 0.72 and an actual overall efficiency of the methanol synthesis section η_{MSS} of about 0.79.

4.1 Alkaline electrolyser

The operating pressure and temperature of the alkaline electrolysis processes were set equal to 5 bar and 65 °C, since under these conditions the efficiency reaches the highest value.

Since for each cell the molar water flow rate is the same as that of hydrogen and the utilisation factor is set to 1, a water flow rate of approximately 640 kg/h is needed for producing the 71.5 kg/h hydrogen stream required by the MSS to obtain the desired methanol production (351 kg/h).

The chemical power of the hydrogen produced by the AEL is equal to 2.3 MW, being the hydrogen LHV equal to 120.0 MJ/kg. Globally, the power absorbed by the AEL, considering also the auxiliaries, is equal to about 3200 kW, corresponding to a specific energy consumption of 44.5 $kWh/kg_{(H2)}$ (about 4 $kWh/Nm^3_{(H2)}$), which is consistent with values reported in the literature [47]. The efficiency of the electrolysis process results equal to 0.722

4.2 Methanol synthesis section

Given the operating conditions of the methanol synthesis section the outlet temperature of the synthesis reactor results equal to about 290 °C, while the products of the reactor are mainly composed of hydrogen (molar fraction slightly lower 0.8), with a minor amount of methanol (0.04). Flash processes increases the methanol concentration in the product up to a value of 49% (crude methanol). The distillation column leads to a methanol purity of 96.4%. Table 4 shows the composition of the outlet of the synthesis reactor, the two flashes (purified bottoms), and the distillation column.

Table 4 Molar composition of the main flow of the synthesis section

Species	Synthesis reactor	Flash 1 (top)	Flash 1 (bottom)	Flash 2 (top)	Flash 2 (bottom)	Distillation column

H_2	0.7770	0.8549	0.0000	0.0002	0.0000	0.0000
CO_2	0.1014	0.0954	0.1612	0.9238	0.0182	0.0360
H_2O	0.0390	0.0010	0.4173	0.0097	0.4937	0.0000
CO	0.0423	0.0464	0.0020	0.0127	0.0000	0.0000
CH_3OH	0.0403	0.0023	0.4194	0.0536	0.4881	0.9640

Since the methanol LHV is equal to 19.9 MJ/kg, the methanol production (351 kg/h) corresponds to a chemical power of 1.94 MW, leading to a chemical energy conversion efficiency $\eta_{MSS,C}$ equal to 0.841. Adding the MSS auxiliaries contribution $P_{BOP,MSS}$, equal to about 155 kW, allows to calculate the actual overall efficiency η_{MSS} (0.788). Globally, an efficiency of the power-to-liquids process η_{PtL}, equal to 0.579 was calculated. The performance indexes of the power-to-liquids section are summarized in Table 5.

Table 5 Performance indexes of the PtL section	
η_{AEL}	0.722
φ_{AEL}	0.954
η_{MSS}	0.788
$\eta_{MSS,C}$	0.841
η_{PtL}	0.579

Due to the intermittency of renewable sources the continuous operating hours of the hydrogen and methanol production plants are not easily quantifiable. With the hypothesis of a 6-hours of RES feeding, a methanol production of about 2.1 tons was calculated, leading to a storage volume of about 2.7 m^3.

4.3 CRGT plant

On the basis of the previous considerations, the influence of temperature, pressure and *n* on the reforming process was analysed under the assumption of thermodynamic equilibrium. The temperature of the reforming process was varied in the range 200–300 °C, while the molar ratio *n* in the range 1-3. Moreover, in order to fulfil the fuel pressure requirements of small-scale gas turbines, two different pressure values, equal to 6 and 12 bar, were considered. Figure 8 shows the methanol conversion rate in function of the reforming temperature for different values of pressure and *n*.

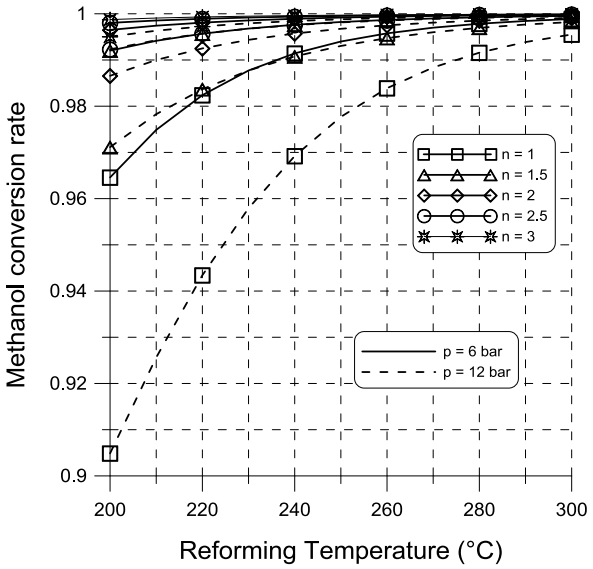

Fig. 8 – Methanol conversion as a function of reforming temperature for different values of reforming pressure and molar ratio *n*.

As appears from the Figure 8, at equilibrium conditions the methanol conversion is very high already at 200 °C, with a lowest value of 92% in case of 12 bar and *n* equal to 1. A temperature increase enhances the methanol conversion, that is almost complete at a reforming temperature of 300 °C, for any value of *n* and pressure (for *n* greater than 1.5 is higher than 99.8%).

Since the thermal energy from gas turbine exhausts is available at high temperature (450-750 °C), a reforming temperature of 300 °C was assumed in this study. As well as the water gas shift conversion reaction, at 300 °C the overall steam reforming reaction is not influenced by the reactor operating pressure since the conversion of methanol is almost complete. Figure 9 shows the molar composition of the reforming gas as a function of the water/methanol molar ratio *n* for a reforming pressure of 6 and 12 bar.

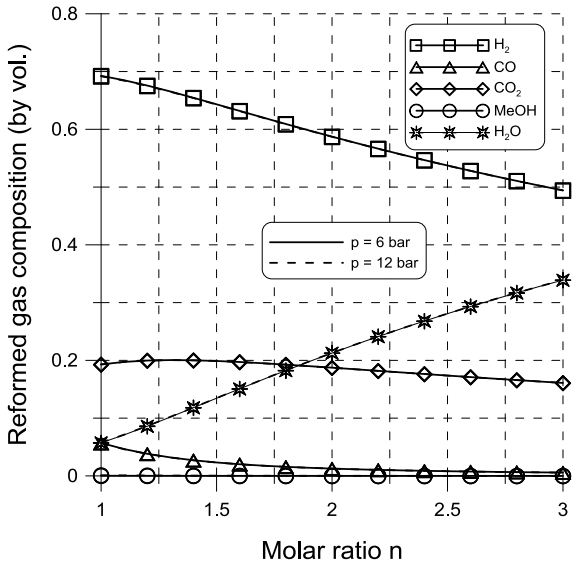

Fig. 9 – Reformed gas composition as a function of molar ratio *n*

The reformed gas is mainly composed of H_2, H_2O, CO, and CO_2, with a negligible methanol concentration. At stoichiometric conditions, the molar concentration of hydrogen is slightly lower than 0.7, whereas CO_2 concentration is slightly lower than 0.2. Both CO and water vapour accounts for about 5-6%. Finally, methanol is practically absent (lower than 0.1%). An increase of *n* results in a greater dilution with water vapour that reaches a molar concentration of about 0.34 for *n* equal to 3. At 300 °C methanol conversion is almost complete also in stoichiometric conditions. Consequently, an increase of *n* simply influences the shift conversion equilibrium, favouring the production of both CO_2 and H_2, and reducing the CO content. In fact, for *n* greater than 2, the reformed gas is only composed of H_2, H_2O and CO_2, and CO content is lower than 1.5%.

A parametric analysis of the CRGT power plant as a function of both the turbine inlet temperature (TIT) and the pressure ratio β was carried out to evaluate the influence on the efficiency of both the gas turbine and the overall system. As previously specified, small-scale gas turbines are characterized by lower values of TIT and pressure ratio than those of industrial scale gas turbines. Therefore, the parametric analysis was limited to 900-1100°C and 5-12, respectively. A variation of the TIT and β strongly influences the temperature at the gas turbine outlet, as appears in Figure 10.

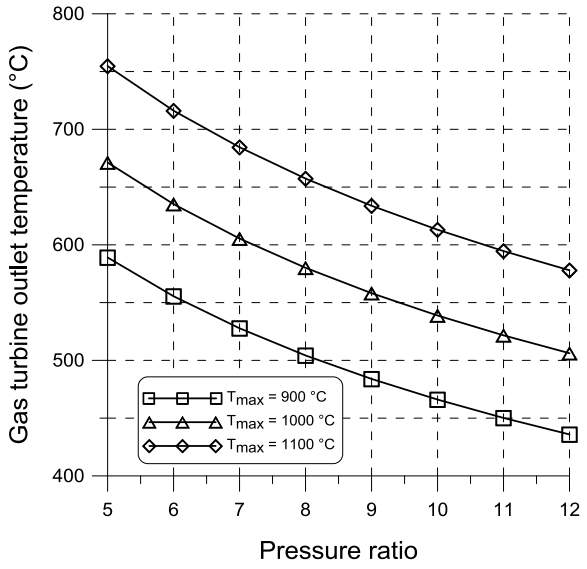

Fig. 10 – Gas turbine outlet temperature as a function of β for different values of TIT

(A higher TIT leads to higher outlet temperature about 70-85 °C each 100 °C of TIT increase). For a set TIT, an increase of β from 5 to 12 reduces the outlet temperature of 150-175 °C, depending on the TIT value. In the range considered in this study, the outlet temperature varies between 435 and 755 °C.

A higher temperature of the gas turbine exhausts increases the thermal energy available for the reforming process. At the same time, the thermal energy available is strictly related to the exhausts flow rate, that is given by the sum of air and water-methanol flow rates. Figure 11 shows both the air and the reformed gas mass flow as a function of β for different values of the TIT.

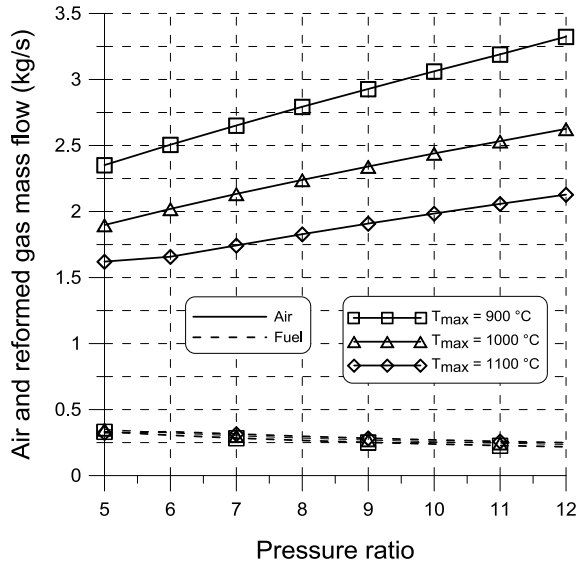

Fig. 11 – Air and reformed gas mass flow as a function of β for different values of TIT

Air and reformed gas show opposite behaviour. Air mass flow decreases with TIT (up to 20% from 900 to 1000 °C), since the chemical power feeding the combustion chamber was assumed to be constant (having set the methanol feeding equal to the MSS production, 351 kg/h). On the contrary, an increase of TIT assures a greater heat available for the reforming process improving the reformed gas production. In addition, the air mass flow increases with the pressure ratio (about 30-40% increasing β from 5 to 12), since the air temperature at the compressor outlet is higher. Conversely, reformed gas flow rate decreases with β, because a lower temperature of the exhausts reduces the heat available for the reforming. Globally, since the air influence is notably more marked than the reformed gas one, the exhausts flow rate decreases with TIT and increases with β.

Having set the methanol feeding in the CRGT, an increase of thermal energy available for the reforming process leads to a greater amount of water vapour to be fed to the CRGT and, consequently, to a greater value of the water/methanol molar ratio *n*. Figure 12 shows the molar ratio *n* as a function of pressure ratio for different values of the TIT.

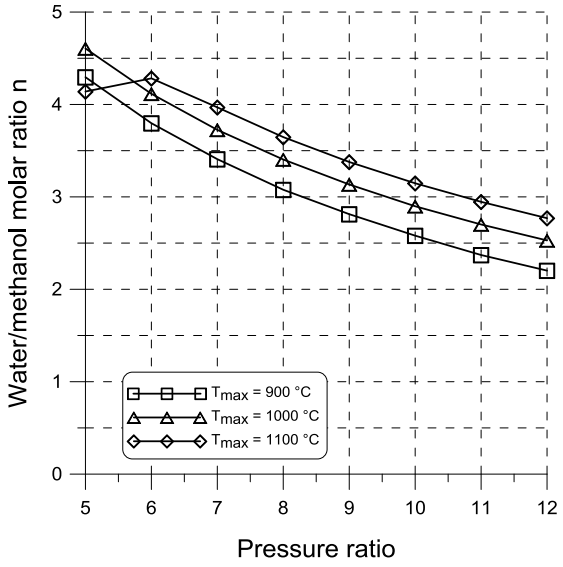

Fig. 12 – Water/methanol molar ratio *n* as a function of β for different values of TIT

Globally, the influence of the gas turbine outlet temperature on the thermal energy available for the reforming is more marked than the one related to the exhausts flow rate. Therefore, the value of *n* increases with TIT and decreases with β. Globally, a *n* value in the range 2.2-4.6 can be obtained for the adopted operating parameters. In particular, a reduction of about 2.0 is noticed increasing β

from 5 to 12, whereas an increase of about 0.25-0.30 can be obtained for each 100 °C of TIT increase. In case of a TIT equal to 1100 °C and β lower than 6, the heat available from the exhausts would lead to a reformed gas production exceeding the maximum increase of 20% in the turbine. Therefore, the heat cannot be fully exploited, leading to a reduction of the *n* value.

Figure 13 shows the CRGT power output as a function of β for different values of the TIT.

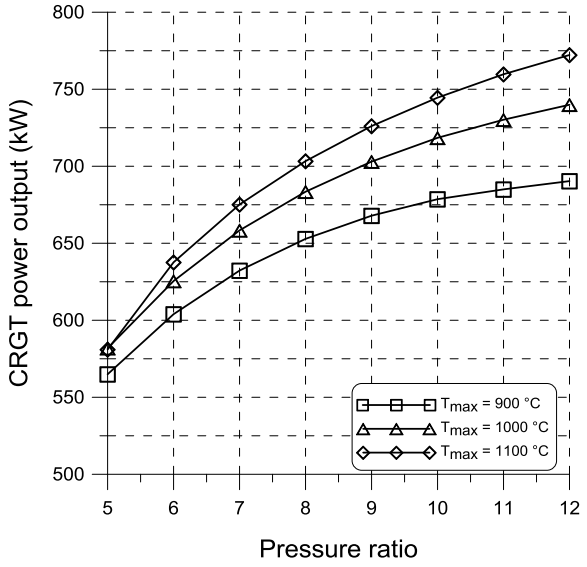

Fig. 13 – CRGT power output as a function of pressure ratio for different values of TIT

As appears from the Figure 13, the power output ranges between 560 and 770 kW, depending on TIT and β values. Indeed, an increase of TIT and β enhances the performance of the gas turbine cycle, leading to a greater power production. The influence of TIT is more marked for the highest values of β. In case of β and TIT equal to 6 and 1100 °C, the reduction of *n* leads to a power output penalization.

Figure 14 shows the CRGT efficiency as a function of β for different values of the TIT. For the sake of comparison, Figure 14 reports also the efficiency of the reference gas turbine in case of natural gas feeding without any reforming section. For comparative purpose, main gas turbine parameters (i.e., compressor and turbine efficiencies, inlet and outlet pressure drop, combustor efficiency and pressure drop, mechanical losses and auxiliaries consumption) were assumed equal for both the analysed cases.

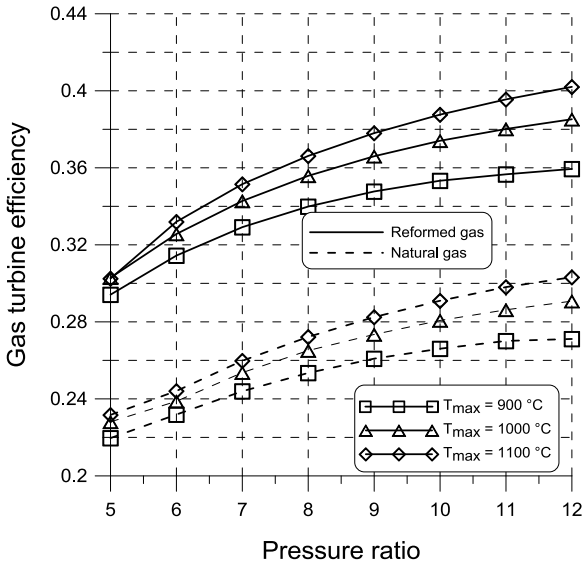

Fig. 14 – Gas turbine efficiency as a function of pressure ratio for different values of TIT

As previously explained for the CRGT power output (Figure 13), an increase of TIT and β favourably influences the CRGT efficiency. Starting from an efficiency of about 0.30 (β = 5), a CRGT efficiency ranging between 0.359 (TIT = 900 °C) and 0.402 (TIT = 1100 °C) can be reached for β equal to 12. As appears from Figure 14, the CRGT efficiency is considerably higher (up to 10 percentage points) than the one of the reference gas turbine fed with methane, thanks to the higher mass flow evolving in the gas turbine.

4.4 CO_2 removal, compression and storage section

The CO_2 capture system based on MEA allows to remove 90% of the CO_2 contained in the exhausts (about 440 kg/h). The influence of both TIT and β on the performance of the CO_2 capture system is negligible, since the CO_2 content in the exhausts is not influenced by TIT and β. The main energy requirement of the section is due to the reboiler duty for the solvent regeneration. A specific thermal energy equal to 3.75 MJ for kg of CO_2 removed was calculated, leading to a regeneration thermal power of about 455 kW. Moreover, the CO_2 compressors require about 43 kW for reaching the storing pressure of 80 bar. At that storing pressure the CO_2 shows a density of about 137 kg/m^3. Since the overall system is designed to operate for 6 hours of discharging phase, about 2600 kg of CO_2 are stored for feeding the MSS section in the following charging phase, requiring a tank of about 38 m^3. Globally, about 520 kg/h of CO_2 are needed for synthesize the methanol, requiring about 80 kg/h from another source. Energy consumptions associated to this further CO_2 feeding are

neglected, imagining a future economy where CCS and CCU are largely diffused and where the CO_2 is captured and available in large quantities, whether it is simply stored following a CCS process or it is purposely stored to be subsequently used in power-to-X applications.

4.5 ORC system

Different sizes for the ORC engine were considered, varying the thermal power available from the CRGT exhausts at the ORC vaporizer. An increase of the ORC size means a higher mass flow rate of the organic fluid, leading to a higher efficiency of the turbine, since it is strongly affected by the organic fluid mass flow. Figure 15 shows the mass flow rate of the organic fluid and the turbine isentropic efficiency as a function of the thermal power available at the ORC vaporizer.

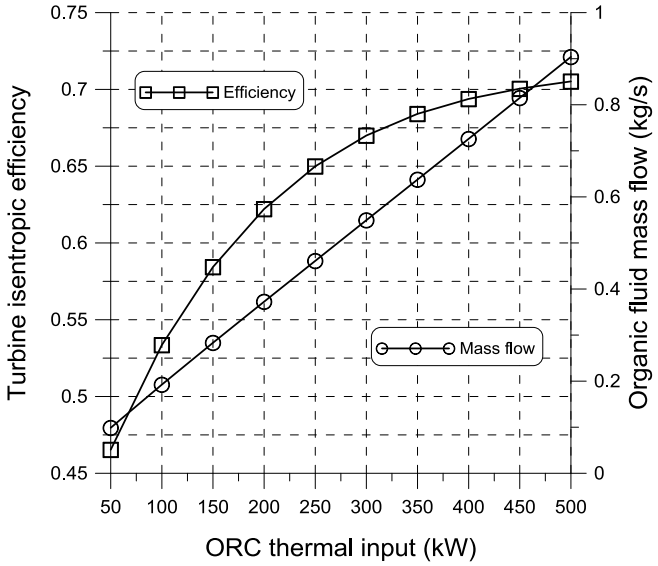

Fig. 15 – Organic fluid mass flow and turbine efficiency as a function of ORC thermal input

The working fluid flow rate increases from about 0.1 kg/s to about 0.9 kg/s increasing the thermal input from 50 to 500 kW. At the same time, the isentropic efficiency of the ORC turbine ranges between 0.46 and 0.70.

Since the main other operating parameters were fixed, the ORC global efficiency is strictly related to the efficiency of the turbine, increasing with the size of the system. Figure 16 shows both the ORC global efficiency and power output as a function of the thermal power available at the ORC vaporizer.

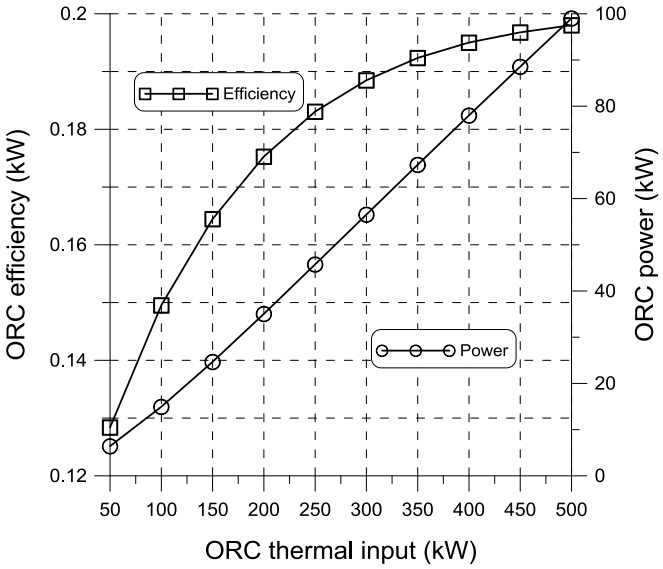

Fig. 16 – ORC global efficiency and power output as a function of ORC thermal input

The ORC system shows a very low global efficiency (lower than 0.13) in case of minor thermal input (50 kW) and the global efficiency quickly increases up to about 0.20 for the maximum size considered in this study (500 kW). At this size, the power output of the ORC system is slightly lower than 80 kW, whereas at the lowest size it is limited to 6 kW.

4.6 CRGT plant plus ORC system

The introduction of the ORC engine reduces the heat available for the reforming process, and, in particular, for preheating, vaporizing and superheating the water-methanol mixture. Figures 17a and 17b show the T-Q diagrams of the CRGT without (a) or with (b) the ORC integration. In particular, Figures 17a and 17b refer to a gas turbine with TIT and β equal to 1000 °C and 8, respectively, and to a ORC thermal input of 300 kW, assumed as reference case.

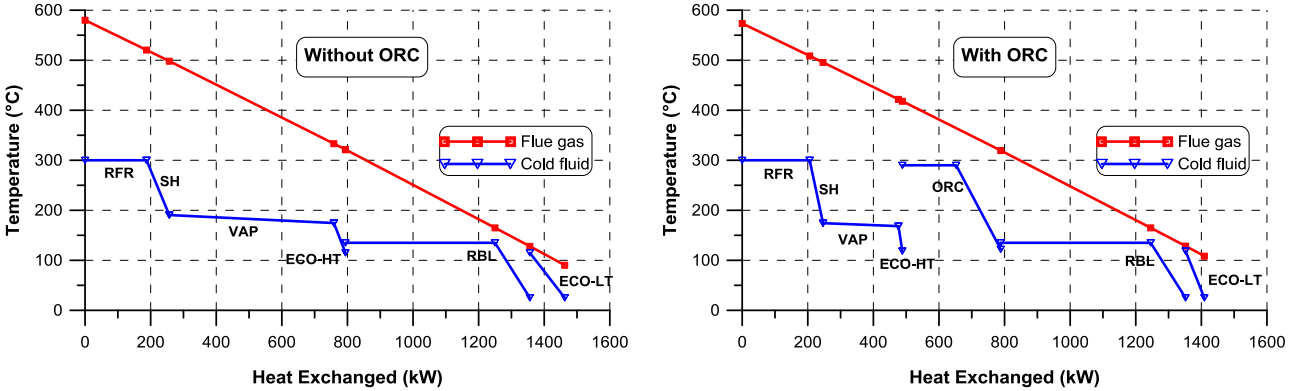

(a) (b)

Fig. 17 – T-Q diagrams of the CRGT

ECO (Economizer), RBL (Reboiler), RFR (Reformer), SH (Superheater), VAP (Vaporizer)

As appears from the Figures 17a and 17b, 1400-1500 kW of thermal power can be recovered from the CRGT exhausts. About 550 kW are required to preheat and vaporize the steam needed for the solvent regeneration in the distillation column (RBL). Without the ORC integration, the remaining heat is fully devoted to preheating, vaporizing, superheating, and reforming the water-methanol mixture, assuring an *n* value of 3.4. The introduction of the ORC engine reduces the heat available for the reforming process. As the methanol feeding was fixed, an increase of the ORC thermal input leads to a reduction of the water flow rate and, consequently, to a lower value of *n* in the reformer (equal to 1.1 for an ORC thermal input of 300 kW, as in Figure 17b). Figure 18 reports the value of *n* as a function of the ORC thermal power input for different values of TIT and β.

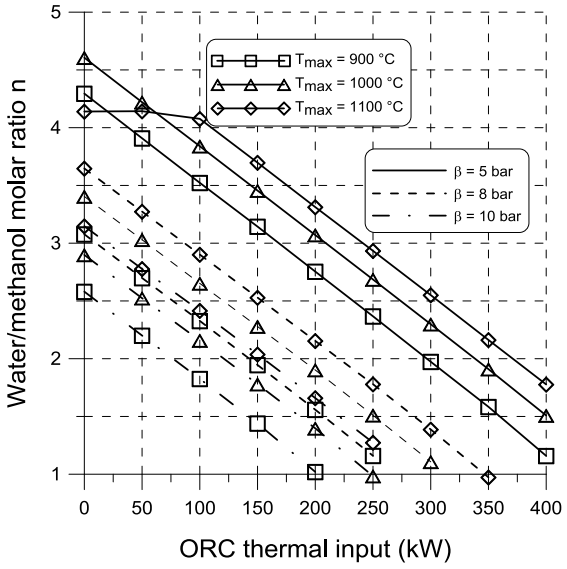

Fig. 18 – Water/methanol molar ratio *n* as a function of ORC thermal input for different values of TIT and β

The increase of the ORC thermal input notably reduces the value of *n*, down to a minimum value assumed equal to 1 (stoichiometric conditions), where the maximum heat available for the ORC is obtained. An ORC thermal input higher than 400 kW can be reached only for β = 5, while for higher values of β the heat available cannot exceed 350 kW.

The reduction of *n* affects the CRGT performance, since it reduces the mass flow rate evolving in the turbine and, as a consequence, the specific work. Subsequently, the introduction of the ORC causes a reduction of the CRGT power output. Figure 19 shows the CRGT power output as a function of the thermal power available for different values of TIT and β.

,

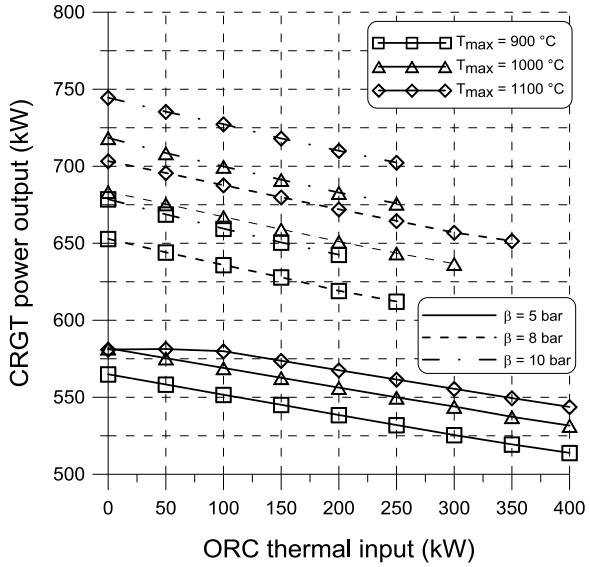

Fig. 19 – CRGT power output as a function of ORC thermal input for different values of TIT and β

As appears from Figure 19, the reduction of CRGT power output is in the order of 30-50 kW for the maximum ORC thermal input. For β equal to 5 and TIT = 900 °C, no power reduction is noticed for an ORC thermal input lower than 100 kW since the heat available from exhausts is too high to respect the limit of 20% mass increase in the gas turbine.

As a matter of fact, the CRGT power reduction, due to the lower flow rate evolving in the turbine, is compensated by the ORC power production, boosting the global electricity production. Figure 20 shows the overall power output (CRGT plus ORC) as a function of the thermal power available for different values of TIT and β.

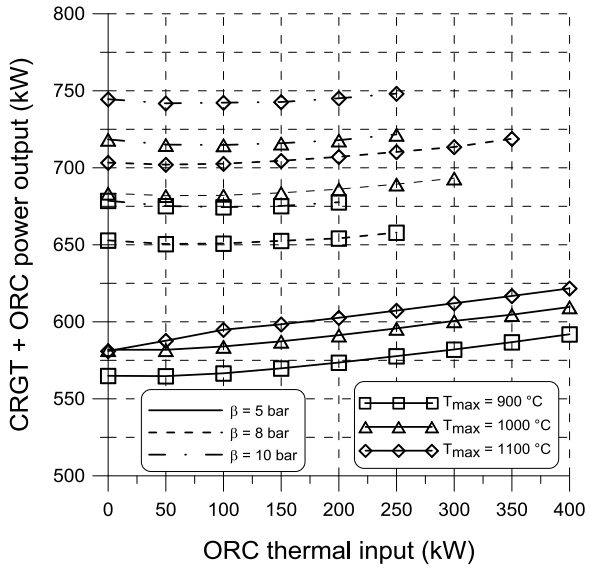

Fig. 20 – Global power as a function of ORC thermal input for different values of TIT and β

As appears from Figure 20, for the lowest values of ORC thermal input the overall power output is reduced. Indeed, the power output of the ORC does not compensate for the CRGT power output reduction since the efficiency of the ORC cycle is particularly low (Figure 16). The increase of organic fluid mass flow allows a greater ORC efficiency leading to a greater overall power output. Globally, for a pressure ratio of 8 or 10, the overall power output ranges between 650 and 750 kW, whereas for β equal to 5, the overall power output exceeds 600 kW only in case of great contribution from the ORC engine.

Finally, the power-to-power efficiency η_g provides an overview of the overall system performance as a function of the operating parameters of the CRGT and ORC. As appears from equations (14) and (15), η_g depends on both the power production and the power-to-liquids processes. The power-to-liquids efficiency η_{PtL}, reported in Table 4 (0.579), should be corrected since a large fraction of the CO_2 needed for the MSS, is available at 80 bar from the CO_2 capture, compression and storage section integrated with the CRGT. The actual efficiency η_{PtL} results equal to 0.587. Figure 21 shows the power-to-power efficiency of the overall system as a function of ORC thermal input for different values of TIT and β.

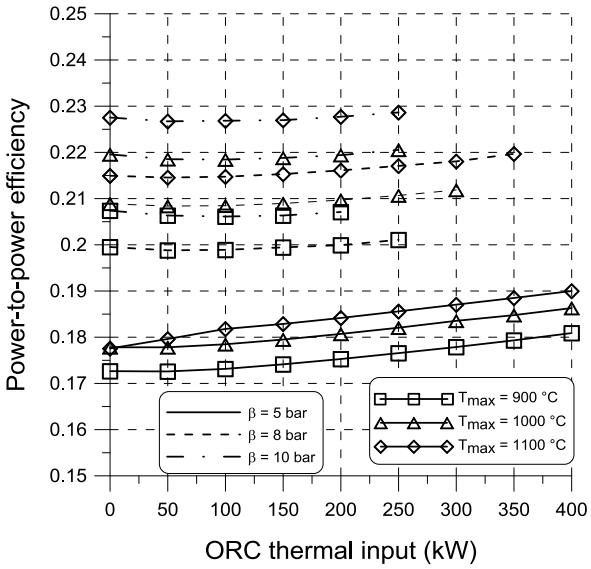

Fig. 21 – Power-to-power efficiency of the overall system as a function of ORC thermal input for different values of TIT and β

The power-to-power efficiency shows the same behaviour than the overall power output reported in Figure 20. Indeed, η_g increases with β and TIT and for great values of the ORC thermal input. A maximum value slightly lower than 0.23 can be obtained with $\beta = 10$ and $\mathrm{TIT} = 1100\ ^{\circ}\mathrm{C}$. Globally, a pressure ratio of 8 or 10 leads to a power-to-power efficiency of the overall system η_g higher than 0.2. Lower values of β limits the power-to-power efficiency in the range 0.17-0.19.

Figure 22 shows the flow diagram of the entire power-to-power plant, reporting the main mass and energy flows of the overall system for the reference case (β = 8, TIT = 1000 °C and ORC thermal input = 300 kW).

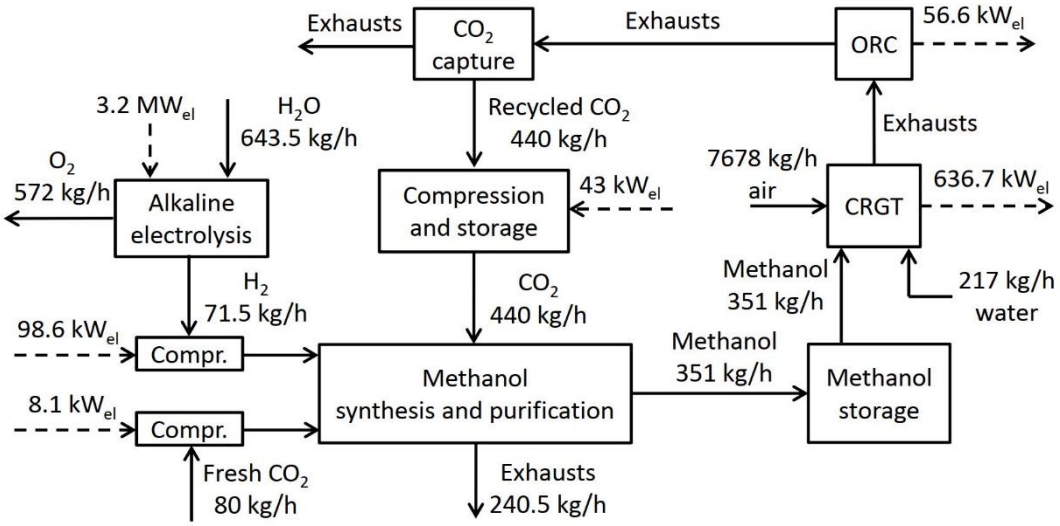

Fig. 22 – Flowsheet of the overall system with mass and energy flows for the reference case

Table 6 summarizes the main results of the overall system in terms of performance indexes and net power of the electricity production sections for the reference case (β = 8, TIT = 1000 °C and ORC thermal input = 300 kW).

Table 6 Main results of the system

	CRGT	CRGT+ORC
P_{CRGT}	683.5 kW	636.7 kW
P_{ORC}	/	56.6 kW
$P_{CRGT+ORC}$	683.5 kW	693.3 kW
η_{CRGT}	0.3558	0.3315
$\eta_{CRGT+ORC}$	0.3558	0.3609
η_g	0.2089	0.2119

5. Conclusions

Renewable energy sources and carbon capture are key solutions to reduce the overall emissions of CO_2 in the atmosphere. In this framework, power-to-X processes are an interesting option to employ renewable energy producing hydrogen and, via CO_2 hydrogenation, chemicals compounds to be used as fuels in energy systems.

In this paper, the integration between a power-to-methanol energy storage system and a chemically recuperated gas turbine (CRGT) plant was studied. The methanol is produced via CO_2 hydrogenation in a methanol synthesis section fed by hydrogen from an alkaline water electrolyser, exploiting renewable energy sources. The CRGT is equipped with a CO_2 capture, compression, and storage system to provide the CO_2 for methanol synthesis. The CRGT can be also integrated with an ORC engine to better exploit the thermal energy from the turbine exhausts.

The power-to-methanol section was sized with reference to a 3.2 MW commercial alkaline electrolyser assuring a hydrogen production of about 800 Nm^3/h and, subsequently, a methanol production of about 350 kg/h (half of the size of the only existing renewable methanol synthesis plant). The chosen configuration leads to an efficiency of the power-to-methanol process slightly lower than 0.6.

The resulting methanol flow rate allows the feeding of a small-scale (several hundred of kW) gas turbine, equipped with a methanol reforming section to enhance the plant performance. Small-scale gas turbines are characterized by low values of both compression ratio (5-12) and maximum temperature (900-1100 °C). A higher TIT leads to a higher temperature of the gas turbine exhausts, increasing the thermal energy available for the reforming process. Globally, the CRGT power output ranges between 560 and 770 kW, depending on TIT and β values. Indeed, an increase of TIT and β enhances the performance of the gas turbine cycle, leading to a greater power production and also to a higher CRGT efficiency (ranging between 0.359 and 0.402 for β equal to 12). A reference case with TIT = 1000 °C and β = 8 was set.

The study demonstrated that CRGT plants can be an interesting low carbon technology for exploiting the renewable methanol. Indeed, despite a power-to-power efficiency of the overall system lower than 0.23, the proposed system can effectively store renewable energy surplus and, then, produce electricity with very low CO_2 emissions. Despite reducing the heat available for the reforming process, the introduction of the ORC allows a better use of the heat released by the CRGT, slightly improving the global efficiency by about 0.3-0.4 percentage points. In fact, the CRGT power reduction, due to the lower flow rate evolving in the turbine, is compensated by the ORC power production, boosting the global electricity production.

Finally, the power-to-power efficiency of the proposed system is significantly lower than that of a similar integrated system, previously studied by the same authors, based on a solid oxide fuel cell (SOFC) that assures a global efficiency in the order of 0.33 (even though the high energy requirements of the CO_2 capture, compression and storage system were not considered). Nevertheless, the CRGT is a significantly less expensive technology than SOFC and assures a remarkably higher reliability. It should be kept in mind that the present analysis is focused on the technical aspect of the proposed system. To evaluate the financial viability of the overall process our future investigations under development will consider a comprehensive economic analysis.

References

[1] Rahman AF, Aziz MA, Saidur R, Bakar AWWA, Hainin MR, Putrajaya R, et al. Pollution to solution: Capture and sequestration of carbon dioxide (CO2) and its utilization as a renewable energy source for a sustainable future. Renew Sustain Energy Rev 2017;71:112–

26. https://doi.org/10.1016/j.rser.2017.01.011.

[2] Mac Kinnon MA, Brouwer J, Samuelsen S. The role of natural gas and its infrastructure in mitigating greenhouse gas emissions, improving regional air quality, and renewable resource integration. Prog Energy Combust Sci 2018;64:62–92. https://doi.org/10.1016/j.pecs.2017.10.002.

[3] Kvamsdal HM, Jordal K, Bolland O. A quantitative comparison of gas turbine cycles with CO2 capture. Energy 2007;32:10–24. https://doi.org/10.1016/j.energy.2006.02.006.

[4] Carapellucci R, Milazzo A. Thermodynamic optimization of a reheat chemically recuperated gas turbine. Energy Convers Manag 2005;46:2936–53. https://doi.org/10.1016/j.enconman.2005.02.007.

[5] Carapellucci R, Risalvato V, Bruno C, Cau G. Performance and emissions of CRGT power generation systems with reformed methanol. Proc. 31st Intersoc. Energy Convers. Eng. Conf., Washington, DC: 1996, p. 707–12. https://doi.org/10.1109/IECEC.1996.553784.

[6] Rostrup-Nielsen JR. Steam reforming and chemical recuperation. Catal Today 2009;145:72–5. https://doi.org/10.1016/j.cattod.2008.06.019.

[7] Liu X, Zheng H, Liu Q. Research of methane reforming and combustion characteristics in chemically recuperated gas turbine. Ind Eng Chem Res 2014;53:1940–6. https://doi.org/10.1021/ie403014c.

[8] Poullikkas A. An overview of current and future sustainable gas turbine technologies. Renew Sustain Energy Rev 2005;9:409–43. https://doi.org/https://doi.org/10.1016/j.rser.2004.05.009.

[9] Cocco D, Tola V, Cau G. Performance evaluation of chemically recuperated gas turbine (CRGT) power plants fuelled by di-methyl-ether (DME). Energy 2006;31. https://doi.org/10.1016/j.energy.2005.05.015.

[10] Duwig C, Nyberg B, Thern M. Efficient operation of a gas turbine on methanol using chemical recuperation. Proc. ASME Turbo Expo 2012 GT2012, 2012, p. 1–9.

[11] Olah GA, Goeppert A, Prakash GKS. Beyond Oil and Gas: The Methanol Economy. 2nd ed. Weinheim, Germany: Wiley-VCH Verlag GmbH & Co. KGaA; 2009.

https://doi.org/10.1002/9783527627806.

[12] de Vasconcelos BR, Lavoie JM. Recent advances in power-to-X technology for the production of fuels and chemicals. Front Chem 2019;7:1–24. https://doi.org/10.3389/fchem.2019.00392.

[13] Galindo Cifre P, Badr O. Renewable hydrogen utilisation for the production of methanol. Energy Convers Manag 2007;48:519–27. https://doi.org/10.1016/j.enconman.2006.06.011.

[14] Ganesh I. Conversion of carbon dioxide into methanol - A potential liquid fuel: Fundamental challenges and opportunities (a review). Renew Sustain Energy Rev 2014;31:221–57. https://doi.org/10.1016/j.rser.2013.11.045.

[15] Bossmann T, Fournié L, Humberset L, Khallouf P. METIS Study S8 - The role and potential of Power-to-X in 2050. 2018. https://doi.org/10.2833/459958.

[16] Sternberg A, Bardow A. Power-to-What?-Environmental assessment of energy storage systems. Energy Environ Sci 2015;8:389–400. https://doi.org/10.1039/c4ee03051f.

[17] Buffo G, Marocco P, Ferrero D, Lanzini A, Santarelli M. Power-to-X and power-to-power routes. Elsevier Inc.; 2019. https://doi.org/10.1016/B978-0-12-814853-2.00015-1.

[18] Koytsoumpa E-I, Bergins C, Buddenberg T, Wu S, Sigurbjörnsson Ó, Tran KC, et al. The Challenge of Energy Storage in Europe: Focus on Power to Fuel. J Energy Resour Technol 2016;138:042002. https://doi.org/10.1115/1.4032544.

[19] Blanco H, Faaij A. A review at the role of storage in energy systems with a focus on Power to Gas and long-term storage. Renew Sustain Energy Rev 2018;81:1049–86. https://doi.org/10.1016/j.rser.2017.07.062.

[20] Denholm P, Ela E, Kirby B, Milligan M. The role of energy storage with renewable electricity generation. Golden, Colorado: 2011.

[21] Duffy P, Fitzpatrick C, Conway T, Lynch RP. Energy Sources and Supply Grids - The Growing Need for Storage. vol. 2019-Janua. 2019. https://doi.org/10.1039/9781788015530-00001.

[22] Zsiborács H, Baranyai NH, Vincze A, Zentkó L, Birkner Z, Máté K, et al. Intermittent renewable energy sources: The role of energy storage in the european power system of

2040. Electron 2019;8. https://doi.org/10.3390/electronics8070729.

[23] Chehade Z, Mansilla C, Lucchese P, Hilliard S, Proost J. Review and analysis of demonstration projects on power-to-X pathways in the world. Int J Hydrogen Energy 2019;44:27637–55. https://doi.org/10.1016/j.ijhydene.2019.08.260.

[24] Kourkoumpas DS, Papadimou E, Atsonios K, Karellas S. ScienceDirect Implementation of the Power to Methanol concept by using CO 2 from lignite power plants : Techno-economic investigation. Int J Hydrogen Energy 2016;41:16674–87. https://doi.org/10.1016/j.ijhydene.2016.07.100.

[25] González-Aparicio I, Pérez-Fortes M, Zucker A, Tzimas E. Opportunities of Integrating CO2 Utilization with RES-E: A Power-to-Methanol Business Model with Wind Power Generation. Energy Procedia 2017;114:6905–18. https://doi.org/10.1016/j.egypro.2017.03.1833.

[26] Adnan MA, Kibria G. Comparative techno-economic and life-cycle assessment of power-to-methanol synthesis pathways. Appl Energy 2020;278:115614. https://doi.org/10.1016/j.apenergy.2020.115614.

[27] Bos MJ, Kersten SRA, Brilman DWF. Wind power to methanol: Renewable methanol production using electricity, electrolysis of water and CO2 air capture. Appl Energy 2020;264:114672. https://doi.org/10.1016/j.apenergy.2020.114672.

[28] Crivellari A, Cozzani V, Dincer I. Design and energy analyses of alternative methanol production processes driven by hybrid renewable power at the offshore Thebaud platform. Energy Convers Manag 2019;187:148–66. https://doi.org/10.1016/j.enconman.2019.03.017.

[29] Crivellari A, Cozzani V, Dincer I. Exergetic and exergoeconomic analyses of novel methanol synthesis processes driven by offshore renewable energies. Energy 2019;187:1–29. https://doi.org/10.1016/j.energy.2019.115947.

[30] Crivellari A, Cozzani V. Offshore renewable energy exploitation strategies in remote areas by power-to-gas and power-to- liquid conversion. Int J Hydrogen Energy 2019;45:2936–53. https://doi.org/10.1016/j.ijhydene.2019.11.215.

[31] Alves LG, Nebra SA. Basic chemically recuperated gas turbines - Power plant optimization

and thermodynamics second law analysis. Energy 2004;29:2385–95. https://doi.org/10.1016/j.energy.2004.03.039.

[32] Liu T, Liu Q, Xu D, Sui J. Performance investigation of a new distributed energy system integrated a solar thermochemical process with chemical recuperation. Appl Therm Eng 2017;119:387–95. https://doi.org/10.1016/j.applthermaleng.2017.03.073.

[33] Cherednichenko O, Havrysh V, Shebanin V, Kalinichenko A, Mentel G, Nakonieczny J. Local green power supply plants based on alcohol regenerative gas turbines: Economic and environmental aspects. Energies 2020;13. https://doi.org/10.3390/en13092156.

[34] Florez-Orrego D, Silva FN, De Oliveria SJ. Syngas production with thermo-chemically recuperated gas expansion systems : An exergy analysis and energy integration study 2019;178. https://doi.org/10.1016/j.energy.2019.04.147 0360-5442/.

[35] Luo C, Zhang N, Lior N, Lin H. Proposal and analysis of a dual-purpose system integrating a chemically recuperated gas turbine cycle with thermal seawater desalination. Energy 2011;36:3791–803. https://doi.org/10.1016/j.energy.2010.11.029.

[36] Pan F, Cheng X, Wu X, Wang X, Luo P. Transient performances of the gas turbine recuperating waste heat through hydrogen rich fuels. Int J Hydrogen Energy 2019. https://doi.org/10.1016/j.ijhydene.2019.02.099.

[37] Su B, Han W, He H, Jin H, Chen Z, Yang S. A biogas-fired cogeneration system based on chemically recuperated gas turbine cycle. Energy Convers Manag 2020;205:112394. https://doi.org/10.1016/j.enconman.2019.112394.

[38] Ni M, Yang T, Xiao G, Ni D, Zhou X, Liu H, et al. Thermodynamic analysis of a gas turbine cycle combined with fuel reforming for solar thermal power generation. Energy 2017;137:20–30. https://doi.org/10.1016/j.energy.2017.06.172.

[39] Van-Dal ÉS, Bouallou C. Design and simulation of a methanol production plant from CO2 hydrogenation. J Clean Prod 2013;57:38–45. https://doi.org/10.1016/j.jclepro.2013.06.008.

[40] Nazerifard R, Khani L, Mohammadpourfard M, Mohammadi-ivatloo B. Design and thermodynamic analysis of a novel methanol, hydrogen, and power trigeneration system based on renewable energy and flue gas carbon dioxide 2021;233.

https://doi.org/10.1016/j.enconman.2021.113922.

[41] Wang L, Zhang Y, Pérez-Fortes M, Aubin P, Lin TE, Yang Y, et al. Reversible solid-oxide cell stack based power-to-x-to-power systems: Comparison of thermodynamic performance. Appl Energy 2020;275:115330. https://doi.org/10.1016/j.apenergy.2020.115330.

[42] Lonis F, Tola V, Cau G. Renewable methanol production and use through reversible solid oxide cells and recycled CO2 hydrogenation. Fuel 2019;246:500–15. https://doi.org/10.1016/j.fuel.2019.02.108.

[43] Lonis F, Tola V, Cau G. Assessment of integrated energy systems for the production and use of renewable methanol by water electrolysis and CO2 hydrogenation. Fuel 2021;285:119160. https://doi.org/10.1016/j.fuel.2020.119160.

[44] Smolinka T. Water Electrolysis: Status and Potential for Development 2014.

[45] Atsonios K, Panopoulos KD, Kakaras E. Investigation of technical and economic aspects for methanol production through CO2 hydrogenation. Int J Hydrogen Energy 2016;41:2202–14. https://doi.org/10.1016/j.ijhydene.2015.12.074.

[46] Bertuccioli L, Chan A, Hart D, Lehner F, Madden B, Standen E. Study on development of water electrolysis in the EU. 2014.

[47] Ursua A, Sanchis P. Static-dynamic modelling of the electrical behaviour of a commercial advanced alkaline water electrolyser. Int J Hydrogen Energy 2012;37:18598–614. https://doi.org/10.1016/j.ijhydene.2012.09.125.

[48] Lonis F. Design, modelling, evaluation and comparison of energy systems for the production and use of renewable methanol using recycled CO2. PhD thesis, University of Cagliari, 2020.

[49] Al-Malah KIM. Aspen Plus®. Hoboken, NJ, USA: John Wiley & Sons, Inc.; 2016. https://doi.org/10.1002/9781119293644.

[50] Boyce MP. 1 - An Overview of Gas Turbines. In: Boyce MPBT-GTEH (Fourth E, editor., Oxford: Butterworth-Heinemann; 2012, p. 3–88. https://doi.org/https://doi.org/10.1016/B978-0-12-383842-1.00001-9.

[51] Leung DYC, Caramanna G, Maroto-Valer MM. An overview of current status of carbon

dioxide capture and storage technologies. Renew Sustain Energy Rev 2014;39:426–43. https://doi.org/10.1016/j.rser.2014.07.093.

[52] Aaron D, Tsouris C. Separation of CO2 from flue gas: A review. Sep Sci Technol 2005;40:321–48. https://doi.org/10.1081/SS-200042244.

[53] Oko E, Wang M, Joel AS. Current status and future development of solvent-based carbon capture. Int J Coal Sci Technol 2017;4:5–14. https://doi.org/10.1007/s40789-017-0159-0.

[54] Macchi E, Astolfi M, editors. Organic Rankine Cycle (ORC) Power Systems. Elsevier; 2017. https://doi.org/10.1016/C2014-0-04239-6.

[55] Quoilin S, Broek M Van Den, Lemort V, Dewallef P, Declaye S. Techno-economic survey of Organic Rankine Cycle (ORC) systems. Renew Sustain Energy Rev 2013;22:168–86. https://doi.org/10.1016/j.rser.2013.01.028.

[56] Benzene | C6H6 - PubChem n.d. https://pubchem.ncbi.nlm.nih.gov/compound/Benzene (accessed March 2, 2020).

[57] Linstrom P. NIST Chemistry WebBook, NIST Standard Reference Database 69. Natl Inst Stand Technol 1997. https://doi.org/https://doi.org/10.18434/T4D303.

[58] Victor RA, Kim JK, Smith R. Composition optimisation of working fluids for organic Rankine cycles and Kalina cycles. Energy 2013;55:114–26. https://doi.org/10.1016/j.energy.2013.03.069.